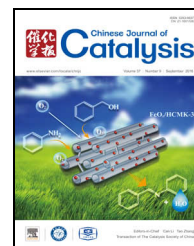


available at [www.sciencedirect.com](http://www.sciencedirect.com)journal homepage: [www.elsevier.com/locate/chnjc](http://www.elsevier.com/locate/chnjc)

## Article

# CoFe<sub>2</sub>O<sub>4</sub>/CdS nanocomposite: Preparation, characterisation, and application in sonocatalytic degradation of organic dye pollutants



Saeed Farhadi\*, Firouzeh Siadatnasab

Department of Chemistry, Lorestan University, Khoramabad 68135-465, Iran

## ARTICLE INFO

## Article history:

Received 16 April 2016

Accepted 14 May 2016

Published 5 September 2016

## Keywords:

CoFe<sub>2</sub>O<sub>4</sub>/CdS nanocomposite

Cadmium dithiocarbamate

Hydrothermal decomposition

Sonocatalyst

Dye degradation

## ABSTRACT

A magnetic CoFe<sub>2</sub>O<sub>4</sub>/CdS nanocomposite was prepared via one-step hydrothermal decomposition of cadmium diethanoldithiocarbamate complex on the surface of CoFe<sub>2</sub>O<sub>4</sub> nanoparticles at a low temperature of 200 °C. The nanocomposite was characterised by X-ray diffraction (XRD), Fourier transform infrared spectroscopy (FT-IR), scanning electron microscopy, energy-dispersive X-ray spectroscopy (EDX), UV-visible spectroscopy, transmission electron microscopy (TEM), N<sub>2</sub> gas sorption analysis, X-ray photoelectron spectroscopy (XPS), and vibrating sample magnetometry. The FT-IR, XRD, EDX and XPS results confirmed the formation of the CoFe<sub>2</sub>O<sub>4</sub>/CdS nanocomposite. Based on the TEM analysis, the CoFe<sub>2</sub>O<sub>4</sub>/CdS nanocomposite constituted nearly uniform, sphere-like nanoparticles of ~20 nm in size. The optical absorption spectrum of the CoFe<sub>2</sub>O<sub>4</sub>/CdS nanocomposite displayed a band gap of 2.21 eV, which made it a suitable candidate for application in sono/photocatalytic degradation of organic pollutants. Accordingly, the sonocatalytic activity of the CoFe<sub>2</sub>O<sub>4</sub>/CdS nanocomposite was evaluated towards the H<sub>2</sub>O<sub>2</sub>-assisted degradation of methylene blue, rhodamine B, and methyl orange under ultrasonic irradiation. The nanocomposite displayed excellent sonocatalytic activity towards the degradation of all dyes examined—the dyes were completely decomposed within 5–9 min. Furthermore, a comparison study revealed that the CoFe<sub>2</sub>O<sub>4</sub>/CdS nanocomposite is a more efficient sonocatalyst than pure CdS; thus, adopting the nanocomposite approach is an excellent means to improve the sonoactivity of CdS. Moreover, the magnetic properties displayed by the CoFe<sub>2</sub>O<sub>4</sub>/CdS nanocomposite allow easy retrieval of the catalyst from the reaction mixture for subsequent uses.

© 2016, Dalian Institute of Chemical Physics, Chinese Academy of Sciences.

Published by Elsevier B.V. All rights reserved.

## 1. Introduction

Organic dye wastewater has become a major source of water pollution. Furthermore, exposure to discharged organic dyes is known to present potential health risks to humans. Accordingly, this issue has attracted considerable attention, and extensive and intensive research studies have been conducted to address it [1–3]. Specifically, different treatment technologies, including biological methods, adsorption, electrochemical processes, membrane technologies, and oxidation processes,

have been developed for the treatment of organic dye wastewater [4–9]. However, most of the above-listed methods have one or more disadvantages such as high cost, low recyclability, complex operations, and complicated designs. Therefore, exploring an alternative, simple, cost-effective, and green approach to addressing organic dye pollution is important.

Photocatalytic degradation is regarded as a promising technology for organic dye treatment in wastewater owing to its high oxidation capabilities and environmental friendliness [10,11]. Among various semiconductor photocatalysts, cad-

\* Corresponding author. Tel: +98-6633120611; Fax: +98-6633120618; E-mail: [sfarhadi1348@yahoo.com](mailto:sfarhadi1348@yahoo.com)

mium sulfide (CdS), with a band gap of 2.4 eV, is one of the most important semiconductors and has been extensively studied in diverse applications, particularly in visible light-driven photocatalysis over the past decades [12–19]. However, rapid recombination of the excited electron-hole pairs considerably limits the photocatalytic efficiency of CdS [13]. Furthermore, when employed in photocatalytic reactions in aqueous media, CdS is susceptible to photocorrosion and oxidation by the photogenerated holes [12,14–17]. To overcome these problems, several approaches have been developed including combining CdS with other semiconductors [14,18,20], noble metals [21], conductive polymers [22], or carbon nanomaterials [23,24]. In recent years, the combination of CdS with magnetic nanomaterials, such as  $\text{Fe}_3\text{O}_4$ ,  $\alpha\text{-Fe}_2\text{O}_3$ , and  $\text{ZnFe}_2\text{O}_4$ , has proven to successfully increase the catalytic activity, photocorrosion resistance, recovery, and reuse of CdS catalyst [25–31]. However, dye wastewater is typically non-transparent and highly concentrated. Consequently, light penetration is limited to only several millimetres, thereby affecting the efficacy of semiconductor nanocomposites to achieve complete photocatalytic degradation of such wastewater. To meet the fast-developing water treatment requirements, there is a great need to devise innovative technologies and materials for efficient removal of pollutants from non-transparent wastewater. As a potential candidate, semiconductor-based sonocatalysis can overcome the above-mentioned disadvantages of the photocatalytic technology because ultrasonic irradiation has a strong penetration ability in all types of water media [32–38]. It is well known that the sonocatalytic efficiency depends highly on the type of catalyst. Therefore, the development of novel sonocatalysts is important to further understand the sonocatalytic mechanism and promote sonocatalysis-based applications.

In the present study, a  $\text{CoFe}_2\text{O}_4/\text{CdS}$  nanocomposite was prepared, for the first time, by a facile, one-step hydrothermal decomposition of cadmium diethanoldithiocarbamate ( $\text{Cd}(\text{DEDTC})_2$ ) precursor over magnetic  $\text{CoFe}_2\text{O}_4$  nanoparticles. The sonocatalytic activity of the  $\text{CoFe}_2\text{O}_4/\text{CdS}$  nanocomposite towards the degradation of organic pollutants, such as methylene blue (MB), rhodamine B (RhB), and methyl orange (MO), was studied under ultrasound irradiation. The effect of different parameters on the efficiency of the process i.e.,  $\text{H}_2\text{O}_2$  amount and catalyst dosage was investigated. Additionally, the activity of the  $\text{CoFe}_2\text{O}_4/\text{CdS}$  nanocomposite was compared with that of pure CdS under similar conditions. To our knowledge, there are no reports on the use of nanocomposites for the rapid sonodegradation of organic dyes, especially in the presence of  $\text{H}_2\text{O}_2$  as an environmentally friendly oxidising agent.

## 2. Experimental

### 2.1. Materials and characterisation

Cadmium nitrate tetrahydrate ( $\text{Cd}(\text{NO}_3)_2 \cdot 4\text{H}_2\text{O}$ ), diethanolamine ( $\text{C}_4\text{H}_{11}\text{NO}_2$ ), and carbon disulphide ( $\text{CS}_2$ ) were provided by Sigma-Aldrich. Iron nitrate nonahydrate ( $\text{Fe}(\text{NO}_3)_3 \cdot 9\text{H}_2\text{O}$ ), cobalt nitrate hexahydrate ( $\text{Co}(\text{NO}_3)_2 \cdot 6\text{H}_2\text{O}$ ), MO ( $\text{C}_{14}\text{H}_{14}\text{N}_3\text{NaO}_3\text{S}$ ), MB ( $\text{C}_{16}\text{H}_{18}\text{ClN}_3\text{S}$ ), and RhB ( $\text{C}_{28}\text{H}_{31}\text{ClN}_2\text{O}_3$ )

were purchased from Merck Chemical Company.

X-ray diffraction (XRD) patterns were recorded on a Rigaku D-max C III X-ray diffractometer using Ni-filtered  $\text{Cu } K_\alpha$  radiation ( $\lambda = 0.15406 \text{ nm}$ ) for the phase determination of the decomposed samples. Infrared spectra were obtained using a Shimadzu Fourier transform infrared (FT-IR) 160 spectrophotometer using KBr pellets. The morphology and elemental analysis of the  $\text{CoFe}_2\text{O}_4/\text{CdS}$  nanocomposite were conducted by scanning electron microscopy-energy-dispersive X-ray spectroscopy (SEM-EDX) on a Mira3 Tescan scanning electron microscope fitted with an energy-dispersive X-ray unit. The size of the nanocomposite particles was determined by transmission electron microscopy (TEM) on an EM10C microscope operating at an accelerating voltage of 100 kV. Optical absorption spectra of the nanocatalysts and dye solutions were recorded on a Cary 100 Conc Varian UV-visible spectrophotometer in the wavelength range of 200–800 nm. For the UV-visible measurements, a homogeneous suspension of the nanocatalyst in ethanol was prepared by sonication for 25 min. The Brunauer-Emmett-Teller (BET) surface area of the nanocomposite was determined by  $\text{N}_2$  adsorption measurements at  $-196^\circ\text{C}$  using a Nova 2000. X-ray photoelectron spectroscopy (XPS; Bestec, Germany) measurements were performed to study the chemical states of the elements. Vibrating sample magnetometry (Meghnatis Daghigh Kavir Co., Iran) was employed to measure the magnetic parameters of the nanocatalysts at room temperature. An ultrasonic apparatus, operating at 37 kHz (Sonic 6MX; output acoustic power = 100 W), was used for the degradation of the dye solutions.

### 2.2. Preparation of the CdS and $\text{CoFe}_2\text{O}_4$ nanoparticles

Diethanoldithiocarbamic acid was prepared from diethanolamine (0.02 mol) and carbon disulphide (0.02 mol) in ethanol (20 mL) under ice-cold conditions ( $5^\circ\text{C}$ ). An aqueous solution of  $\text{Cd}(\text{NO}_3)_2 \cdot 4\text{H}_2\text{O}$  (3.08 g, 0.01 mol) was added to the yellow dithiocarbamic acid solution under continuous stirring. The obtained  $\text{Cd}(\text{DEDTC})_2$  was filtered, washed with alcohol, and dried.

To prepare the CdS nanoparticles,  $\text{Cd}(\text{DEDTC})_2$  (0.5 g) precursor was introduced into a Teflon-lined stainless steel autoclave (50 mL), to which distilled water (30 mL) was added. The autoclave was sealed and maintained at  $200^\circ\text{C}$  for 24 h. Then it was cooled to room temperature. The as-formed yellowish precipitates were filtered and washed with distilled water and ethanol thrice to eliminate any unreacted precursor or by-products.

To prepare the  $\text{CoFe}_2\text{O}_4$  nanoparticles,  $\text{Co}(\text{NO}_3)_2 \cdot 6\text{H}_2\text{O}$  (0.62 g) and  $\text{Fe}(\text{NO}_3)_3 \cdot 9\text{H}_2\text{O}$  (1.71 g) were added to deionised water (25 mL). The solution was stirred for 1 h at room temperature. Then, NaOH aqueous solution (1 mol/L) was supplemented to the suspension to achieve  $\text{pH} = 11$  while stirring for 1 h. A hydrothermal treatment at  $180^\circ\text{C}$  for 12 h was subsequently conducted. The resulting black product was washed with deionised water and ethanol.

### 2.3. Preparation of the $\text{CoFe}_2\text{O}_4/\text{CdS}$ nanocomposite

The synthesised  $\text{CoFe}_2\text{O}_4$  nanoparticles (0.16 g) were dispersed in deionised water (30 mL) and ultrasonicated for 1 h. Then,  $\text{Cd}(\text{DEDTC})_2$  (0.3 g) was added to the  $\text{CoFe}_2\text{O}_4$  suspension. The suspension was ultrasonicated for another hour and then autoclaved in a 50-mL Teflon-lined stainless steel autoclave at 200 °C for 24 h under autogenous pressure. The product was washed with water after cooling to room temperature and then filtered.

#### 2.4. Sonocatalytic tests

The sonocatalytic degradation of the aqueous dye solutions was examined in the presence of  $\text{CoFe}_2\text{O}_4/\text{CdS}$  catalyst powder under 37-kHz ultrasonic irradiation. The reactions were conducted in an open Pyrex cylindrical glass vessel containing  $\text{CoFe}_2\text{O}_4/\text{CdS}$  sonocatalyst (0.5 g/L),  $\text{H}_2\text{O}_2$  (30 mmol/L), and the dye solution (50 mL, 25 mg/L). First, the suspensions were magnetically stirred in the dark for 30 min to achieve adsorption-desorption balance between the dye and sonocatalyst. Then, ultrasonic irradiation was applied to the reaction mixture. All the tests were conducted at room temperature and ambient pressure. During the sonocatalytic reaction, sample aliquots were collected in the determined time intervals, and the catalyst was separated from the suspension by an external magnetic field. The residual MB, RhB, and MO concentrations were determined by UV-visible spectroscopy at 663, 557, and 462 nm, respectively. The dye conversion was calculated as follows:  $(C_0 - C)/C_0$ , where  $C$  is the concentration of the dye after irradiation and  $C_0$  is the concentration of the dye after adsorption equilibrium (before irradiation). The effect of operational parameters on the sonocatalytic activity of the  $\text{CoFe}_2\text{O}_4/\text{CdS}$  nanocomposite i.e., the amount of  $\text{H}_2\text{O}_2$  (0–40 mmol/L), sonocatalyst dosage (0–0.75 g/L), and initial dye concentration (5–35 mg/L) was studied.

### 3. Results and discussion

#### 3.1. Characterisation of the sonocatalyst

The XRD patterns of  $\text{CoFe}_2\text{O}_4$ , CdS, and  $\text{CoFe}_2\text{O}_4/\text{CdS}$  are presented in Fig. 1. As observed in the XRD pattern of  $\text{CoFe}_2\text{O}_4$ , all diffraction peaks could be assigned to spinel-type  $\text{CoFe}_2\text{O}_4$  (JCPDS Card No. 01-1121). The diffraction pattern of CdS showed the presence of both hexagonal and cubic phases (JCPDS Card Nos. 75-1545 and 10-0454, respectively). The XRD pattern of the  $\text{CoFe}_2\text{O}_4/\text{CdS}$  nanocomposite is shown in Fig. 1(c). Comparison of the XRD patterns in Fig. 1(c) and Fig. 1(a), (b) confirmed that the nanocomposite was composed of  $\text{CoFe}_2\text{O}_4$  and CdS phases. The peaks at  $2\theta = 24.88^\circ$ ,  $26.58^\circ$ ,  $28.25^\circ$ ,  $43.86^\circ$ ,  $47.92^\circ$ ,  $51.97^\circ$ , and  $66.97^\circ$  were assigned to the (100), (002), (101), (110), (103), (200), and (203) planes of the hexagonal structure of CdS (JCPDS Card No. 41-1049). The peaks at  $2\theta = 29.96^\circ$ ,  $35.46^\circ$ ,  $43.86^\circ$ ,  $57.05^\circ$ , and  $62.47^\circ$  were assigned to the (220), (311), (400), (511), and (440) planes of the cubic structure of  $\text{CoFe}_2\text{O}_4$  (JCPDS Card No. 01-1121). The diffraction peaks were broader because of the small size effect of the nanocomposite. The average size of the nanocomposite

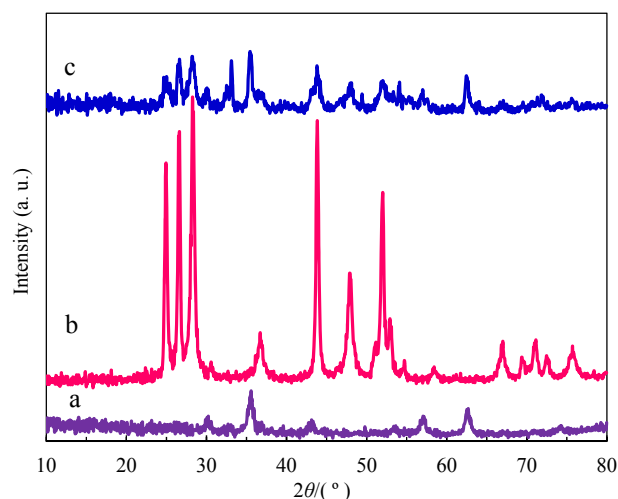


Fig. 1. XRD patterns of (a)  $\text{CoFe}_2\text{O}_4$ , (b) CdS and (c)  $\text{CoFe}_2\text{O}_4/\text{CdS}$ .

particles was  $\sim 20$  nm, as estimated by the Debye-Scherrer equation [39]:  $D_{\text{XRD}} = 0.9\lambda/(\beta\cos\theta)$ , where  $D_{\text{XRD}}$  is the average crystallite size,  $\lambda$  is the wavelength of  $\text{Cu K}\alpha$  radiation,  $\beta$  is the full-width at half-maximum of the chosen diffraction peak, and  $\theta$  is the Bragg angle.

Fig. 2(a) shows the FT-IR spectrum of pure  $\text{CoFe}_2\text{O}_4$ , which displayed two principal absorption bands below  $1000\text{ cm}^{-1}$ , a characteristic feature of all ferrites [40]. Fig. 2(b) illustrates the FT-IR spectrum of the CdS nanoparticles produced via hydrothermal decomposition of  $\text{Cd}(\text{DEDTC})_2$  complex at 200 °C. The bands associated with the complex were no longer apparent, thus indicating the high purity of the product [41]. Fig. 2(c) shows the FT-IR spectrum of the  $\text{CoFe}_2\text{O}_4/\text{CdS}$  nanocomposite, which displayed two main absorption bands below  $1000\text{ cm}^{-1}$ . These bands could be related to the  $\text{CoFe}_2\text{O}_4$  nanoparticles in the nanocomposite [42].

The morphology of the  $\text{CoFe}_2\text{O}_4/\text{CdS}$  nanocomposite was examined by SEM, as shown in Fig. 3. The SEM images show that the  $\text{CoFe}_2\text{O}_4/\text{CdS}$  nanocomposite constituted fine, loosely aggregated, sphere-like nanoparticles with high porosity.

Fig. 4 shows TEM images of the  $\text{CoFe}_2\text{O}_4/\text{CdS}$  nanocomposite. As deduced from the TEM analysis, the particle size distri-

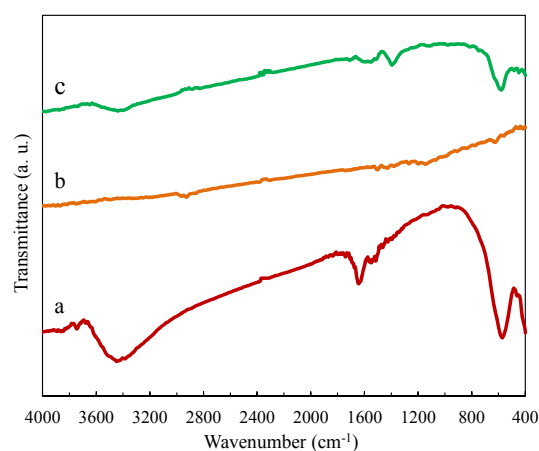


Fig. 2. FT-IR spectra of (a)  $\text{CoFe}_2\text{O}_4$ , (b) CdS and (c)  $\text{CoFe}_2\text{O}_4/\text{CdS}$ .

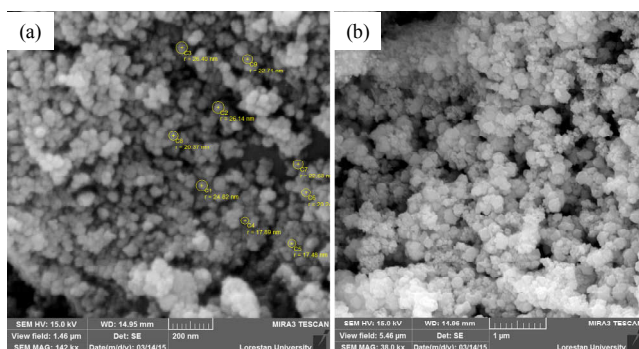


Fig. 3. SEM images of the CoFe<sub>2</sub>O<sub>4</sub>/CdS nanocomposite.

bution was narrow, ranging from 10 to 30 nm, and the mean particle diameter was ~20 nm. These results were consistent with the average particle size calculated by the Debye–Scherrer formula from the XRD pattern.

Additionally, the chemical purity and stoichiometry of the CoFe<sub>2</sub>O<sub>4</sub>/CdS nanocomposite were determined by EDX analysis. The EDX spectrum in Fig. 5 revealed the presence of Cd, S, Co, Fe, and O in the CoFe<sub>2</sub>O<sub>4</sub>/CdS nanocomposite.

The UV-visible absorption spectra of the CdS nanoparticles and CoFe<sub>2</sub>O<sub>4</sub>/CdS nanocomposite are shown in Fig. 6. When compared with the spectrum of the pure CdS sample, that of the CoFe<sub>2</sub>O<sub>4</sub>/CdS composite displayed spectral features that were shifted to the visible light region. The following equation is typically used to calculate the optical absorption near the band edge of a semiconductor [43]:  $(\alpha h\nu)^2 = K(h\nu - E_g)$ , where  $\alpha$ ,  $h$ ,  $\nu$ ,  $E_g$ , and  $K$  are the optical absorption coefficient, Planck constant, light frequency, band gap energy, and a constant relative to the material, respectively. The band gap can be estimated by extrapolating the linear region in the plot of  $(\alpha h\nu)^2$  versus photon energy ( $h\nu$ ). As shown in the inset of Fig. 6, the calculated  $E_g$  of the CoFe<sub>2</sub>O<sub>4</sub>/CdS nanocomposite was ~2.21 eV. This value

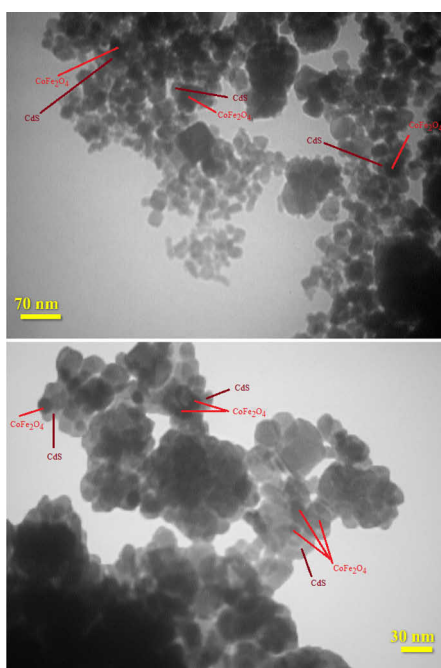


Fig. 4. TEM images of the CoFe<sub>2</sub>O<sub>4</sub>/CdS nanocomposite.

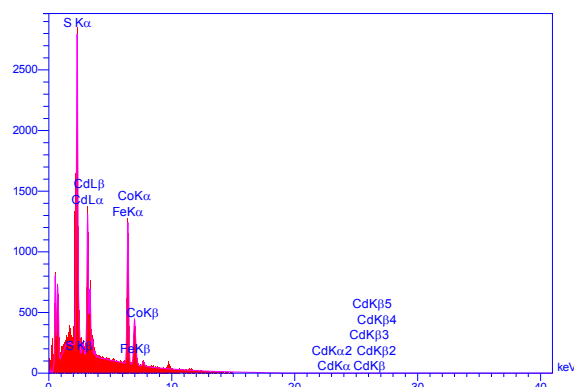


Fig. 5. EDX analysis of the CoFe<sub>2</sub>O<sub>4</sub>/CdS nanocomposite.

suggests that the as-synthesised CoFe<sub>2</sub>O<sub>4</sub>/CdS nanocomposite has a suitable  $E_g$  for application in the catalytic degradation of organic pollutants under visible light. The decrease in the band gap of the CoFe<sub>2</sub>O<sub>4</sub>/CdS nanocomposite (2.21 eV) when compared with CdS nanoparticles (2.37 eV) may be ascribed to the presence of the CoFe<sub>2</sub>O<sub>4</sub> ferrite.

The magnetic behaviours of CoFe<sub>2</sub>O<sub>4</sub>/CdS and CoFe<sub>2</sub>O<sub>4</sub> at room temperature were also investigated. As seen in Fig. 7, the nanocomposite displayed a ferromagnetic behaviour. The coercive force ( $H_c$ ), saturation magnetisation ( $M_s$ ), and remanent magnetisation ( $M_r$ ) of CoFe<sub>2</sub>O<sub>4</sub>/CdS were compared with those of CoFe<sub>2</sub>O<sub>4</sub> in the inset of Fig. 7. As observed, the  $H_c$ ,  $M_s$ , and  $M_r$  values of CoFe<sub>2</sub>O<sub>4</sub>/CdS were smaller than those of CoFe<sub>2</sub>O<sub>4</sub> owing to the presence of non-magnetic CdS [44].

The porosity and specific surface area were determined using the Barrett–Joyner–Halenda method and the BET equation, respectively. The calculated BET surface area of the nanocomposite was 39.329 m<sup>2</sup>/g [45,46]. The pore size distribution of the nanocomposite was centred at ~15.5 nm. The mesoporous structure and relatively high surface area are expected to offer high catalytic activity.

The chemical composition and electronic structure of the synthesised CoFe<sub>2</sub>O<sub>4</sub>/CdS were analysed by XPS. As observed in Fig. 8(a), the survey spectrum of CoFe<sub>2</sub>O<sub>4</sub>/CdS displayed peaks

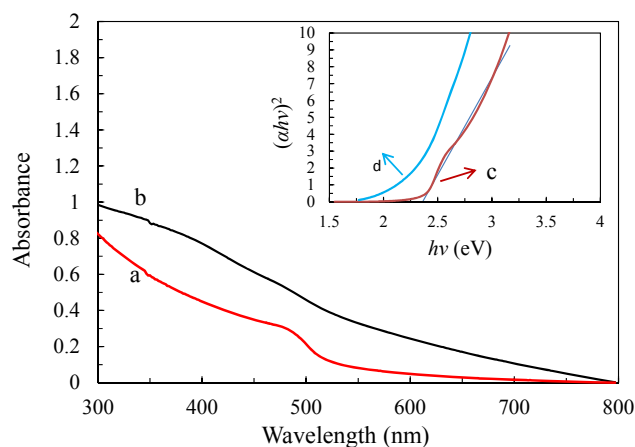
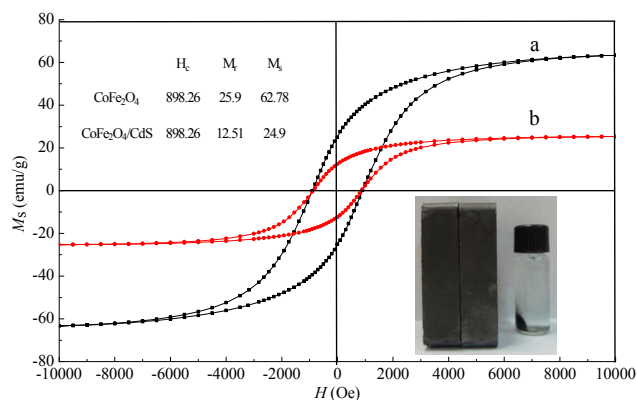


Fig. 6. UV-Vis spectra of (a) CdS nanoparticles and (b) CoFe<sub>2</sub>O<sub>4</sub>/CdS nanocomposite. The inset shows the  $(\alpha h\nu)^2$ – $h\nu$  curves of (c) CdS nanoparticles and (d) CoFe<sub>2</sub>O<sub>4</sub>/CdS nanocomposite.



**Fig. 7.** Room-temperature magnetization curves of (a) CoFe<sub>2</sub>O<sub>4</sub> and (b) CoFe<sub>2</sub>O<sub>4</sub>/CdS nanocomposite. The inset shows the solution after magnetic separation using an external magnetic.

of Cd, S, Co, Fe, and O. The peaks at 406.5 eV ( $3d_{5/2}$ ), 413 eV ( $3d_{3/2}$ ), and 162.7 eV (S  $2p$ ) in the Cd ( $3d$ ) and S ( $2p$ ) XPS scans (Fig. 8(b), (c)) confirmed the presence of Cd<sup>2+</sup> and S<sup>2-</sup> in the form of CdS. The Co  $2p$  XPS spectrum (Fig. 8(d)) featured a main peak at 782.1 eV ( $2p_{3/2}$ ) along with the characteristic satellite peak at 789.2 eV. The presence of the broad satellite peak confirmed the +2 oxidation state of Co element. Similarly, the Fe  $2p$  XPS spectrum (Fig. 8(e)) displayed peaks centred at 713 eV ( $2p_{3/2}$ ) and 726.5 eV ( $2p_{1/2}$ ), thereby confirming the +3 oxidation state of Fe element. The O  $1s$  XPS spectrum (Fig. 8(f)) displayed a broad peak at ~532.1 eV, which corresponds to lattice oxygen in the CoFe<sub>2</sub>O<sub>4</sub> matrix [47].

### 3.2. Sonocatalytic degradation of dyes over the CoFe<sub>2</sub>O<sub>4</sub>/CdS nanocomposite

MB, RhB, and MO were selected as models of organic pollu-

ants to evaluate the sonocatalytic performance of the CoFe<sub>2</sub>O<sub>4</sub>/CdS nanocomposite in the presence of H<sub>2</sub>O<sub>2</sub>. Accordingly, a series of sonocatalytic experiments were conducted. As observed in Fig. 9(a), the intensity of the MB absorption peak at 663 nm decreased as the reaction proceeded and disappeared after 5 min, thus indicating the high sonocatalytic performance of the CoFe<sub>2</sub>O<sub>4</sub>/CdS nanocomposite. The concentration changes ( $C/C_0$ ) of MB at 663 nm as a function of irradiation time under different conditions are shown in Fig. 9(b). Curve (I) in Fig. 9(b) shows that negligible amounts of MB degraded in the presence of ultrasonic irradiation only. Curves (II)–(VI) in Fig. 9(b) show that the degradation percentages of MB in the presence of H<sub>2</sub>O<sub>2</sub> only, and CoFe<sub>2</sub>O<sub>4</sub>/H<sub>2</sub>O<sub>2</sub>, CdS/H<sub>2</sub>O<sub>2</sub>, and CoFe<sub>2</sub>O<sub>4</sub>/CdS systems under ultrasonic irradiation and CoFe<sub>2</sub>O<sub>4</sub>/CdS/H<sub>2</sub>O<sub>2</sub> system without ultrasonic irradiation, were 0.05%, 0.05%, 12%, 15%, and 22%, respectively. Curve (VII) in Fig. 9(b) shows that in the presence of the CoFe<sub>2</sub>O<sub>4</sub>/CdS/H<sub>2</sub>O<sub>2</sub> system, complete degradation (100%) of MB was achieved under ultrasonic irradiation within 5 min. The above results confirmed that the combined use of ultrasonic irradiation, H<sub>2</sub>O<sub>2</sub>, and CoFe<sub>2</sub>O<sub>4</sub>/CdS nanocomposite is necessary to achieve fast and complete degradation of the dyes.

To understand the sonocatalytic degradation kinetic of MB degradation, the pseudo-first-order model [48] was used:  $\ln(C_0/C) = kt$ , where  $C_0$  and  $C$  are the dye concentrations before and after irradiation, respectively,  $k$  is the pseudo-first-order rate constant, and  $t$  is the reaction time. As shown in Fig. 9(c), the  $k$  value for the degradation of MB was 0.77 min<sup>-1</sup>.

To evaluate the scope of this method, the sonocatalytic degradation of RhB and MO was also investigated. As observed from Fig. 10, complete degradation (100%) of both RhB and MO was achieved within 5 and 9 min ( $k = 0.77$  min<sup>-1</sup> and 0.059 min<sup>-1</sup>, respectively). The slow degradation of MO can be related to its high redox potential.

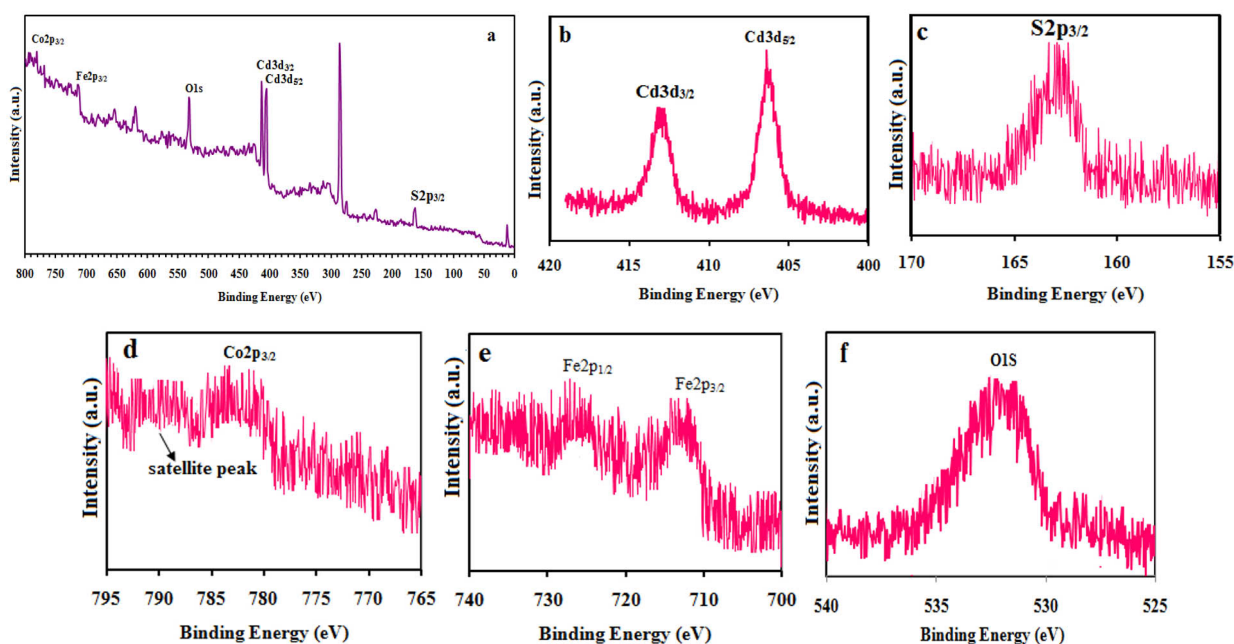


**Fig. 8.** XPS fully scanned spectrum of CoFe<sub>2</sub>O<sub>4</sub>/CdS nanocomposite (a); XPS spectra of Cd  $3d$  (b), S  $2p$  (c), Co  $2p$  (d), Fe  $2p$  (e) and O  $1s$  (f).

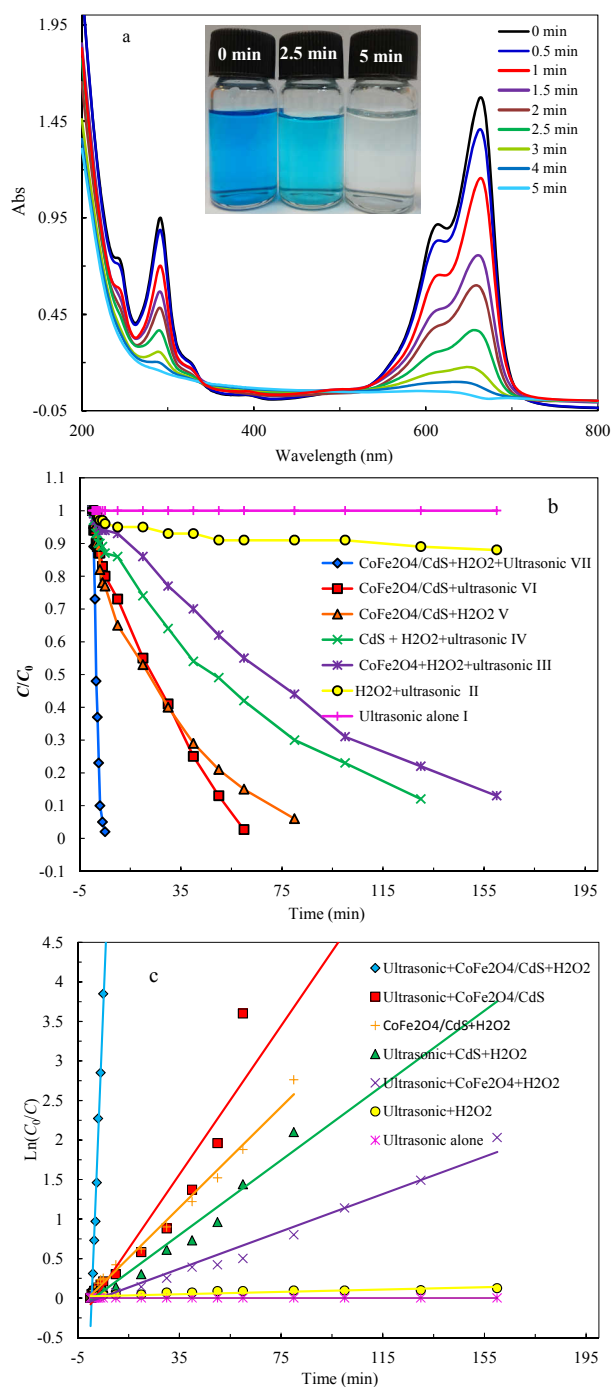


**Fig. 9.** (a) The temporal evolution of MB absorbance spectra in the CoFe<sub>2</sub>O<sub>4</sub>/CdS nanocomposite under ultrasonic irradiation at different intervals. The inset photo shows the colour change of dye solution during irradiation. (b) Concentration changes of MB at 663 nm as a function of irradiation time. (c)  $\ln(C_0/C)$  versus irradiation time in MB solution. Experimental conditions: [MB] = 25 mg/L, [nanocatalyst] = 0.5 g/L [H<sub>2</sub>O<sub>2</sub>] = 30 mmol/L, 25 °C.

Fig. 11 shows the effect of CoFe<sub>2</sub>O<sub>4</sub>/CdS dosage on the sonocatalytic degradation of MB. The degradation of MB was negligible in the absence of the CoFe<sub>2</sub>O<sub>4</sub>/CdS nanocomposite. As the CoFe<sub>2</sub>O<sub>4</sub>/CdS dosage was increased to 0.25 and 0.5 g/L, the sonocatalytic degradation of MB increased to 57% and 100%,

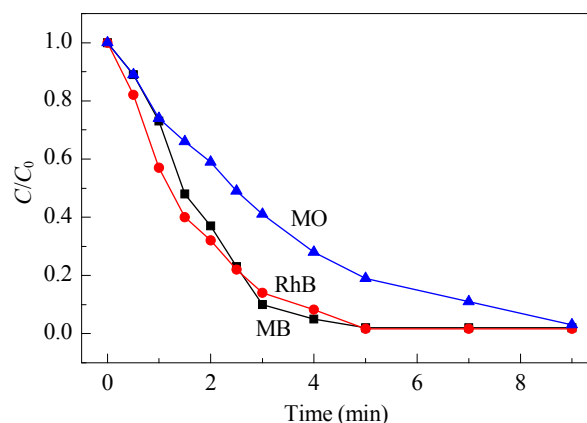


**Fig. 10.** Comparison of the concentration changes of MB, RhB and MO ( $C/C_0$ ) as a function of irradiation time over the CoFe<sub>2</sub>O<sub>4</sub>/CdS nanocomposite. Experimental conditions: [dye] = 25 mg/L, [nanocatalyst] = 0.5 g/L, [H<sub>2</sub>O<sub>2</sub>] = 30 mmol/L, 25 °C, 9 min.

respectively, within 5 min of ultrasonic irradiation. A higher dosage of CoFe<sub>2</sub>O<sub>4</sub>/CdS nanocomposite in the solution provides more active reaction sites for the generation of hydroxyl radicals ( $\cdot\text{OH}$ ), consequently accelerating the degradation rate. Moreover, increasing the sonocatalyst dosage enables the formation of additional nuclei for the cavitation phenomenon, thus generating more  $\cdot\text{OH}$  radicals [49]. However, increasing the CoFe<sub>2</sub>O<sub>4</sub>/CdS nanocomposite dosage further from 0.5 to 0.75 g/L did not increase the degradation rate further. In fact, at the higher dosages, aggregation of the sonocatalyst particles occurred. This phenomenon leads to a reduction in effective surface area and amount of surface active sites for the generation of  $\cdot\text{OH}$  radicals. Moreover, the extent of the cavitation phenomenon is dependent on the active surface area of the sonocatalyst. Thus, in the presence of excess amounts of sonocatalyst, fewer ultrasonic waves circulate in the solution to form cavitation bubbles [50–52].

Additionally, the effect of the amount of H<sub>2</sub>O<sub>2</sub> on catalytic efficiency was investigated under the provided reaction condi-

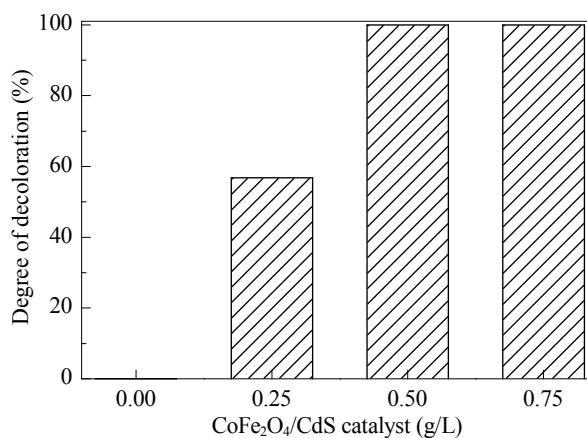


**Fig. 11.** Effect of the CoFe<sub>2</sub>O<sub>4</sub>/CdS dosage on the sonocatalytic degradation of MB. Experimental conditions: [MB] = 25 mg/L, [H<sub>2</sub>O<sub>2</sub>] = 30 mmol/L, 25 °C, 5 min.

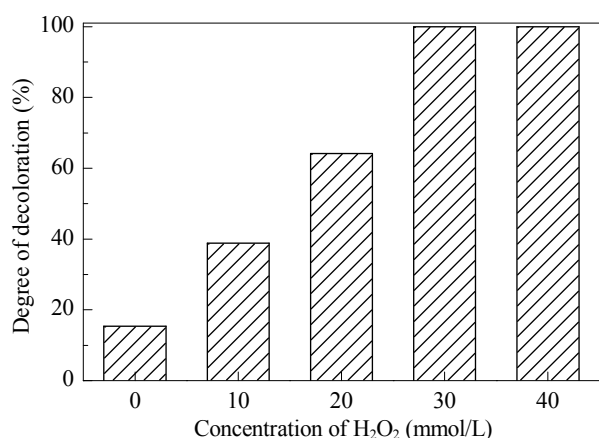
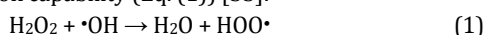


**Fig. 12.** Effect of the H<sub>2</sub>O<sub>2</sub> dosage on the sonocatalytic degradation of MB. Experimental conditions: [dye] = 25 mg/L, [nanocatalyst] = 0.5 g/L, 25 °C, 5 min.

tions, and the results are shown in Fig. 12. As observed, in the absence of H<sub>2</sub>O<sub>2</sub>, only ~15% of MB was degraded. When H<sub>2</sub>O<sub>2</sub> dosage increased from 10 to 30 mmol/L, the degradation efficiency increased correspondingly from 39% to 100%. This degradation rate enhancement was attributed to an increase in •OH as a result of the higher H<sub>2</sub>O<sub>2</sub> dosage. However, increasing the amount of H<sub>2</sub>O<sub>2</sub> further from 30 to 40 mmol/L did not increase the degradation efficiency further—in contrast, it remained rather constant. The excess H<sub>2</sub>O<sub>2</sub> molecules act as a scavenger of •OH to generate perhydroxyl radicals, which have a lower oxidation capability (Eq. (1)) [53]:



Finally, the recyclability of the sonocatalyst was tested (Fig. 13). No significant loss in activity was observed for up to three catalytic cycles, thereby indicating that the as-prepared magnetic sonocatalyst is stable and efficient in the degradation of organic dyes in wastewater.

It is well known that the sonocatalytic degradation of organic pollutants over a sonocatalyst is based on three main phenomena i.e., sonoluminescence, 'hot spot', and oxygen atom escape [37]. Sonoluminescence occurs when a sound wave has sufficient intensity and induces gaseous cavities within a liquid to collapse quickly. These cavities may form pre-existing bubbles or may be generated through a process known as cavitation. Sonoluminescence can be stabilised under laboratory conditions; during this process, a single bubble will periodically expand and collapse continuously while emitting a burst of light at each collapse. Therefore, ultrasonic irradiation results in sonoluminescence and the production of abundant visible light. Visible light has a relatively wide wavelength range because of acoustic cavitations. Both CdS and CoFe<sub>2</sub>O<sub>4</sub> can be excited by visible light to produce sonogenerated carriers and excited holes. The excited-state electrons in the conduction band (CB) of CdS can be readily injected into the CB of CoFe<sub>2</sub>O<sub>4</sub>. Simultaneously, the sonogenerated holes in the valence band (VB) of CoFe<sub>2</sub>O<sub>4</sub> are able to move easily to the VB of CdS. Thus, the sonogenerated electrons and holes move in opposite directions while reducing the recombination probability and enhancing charge separation efficiency, thereby leading to a

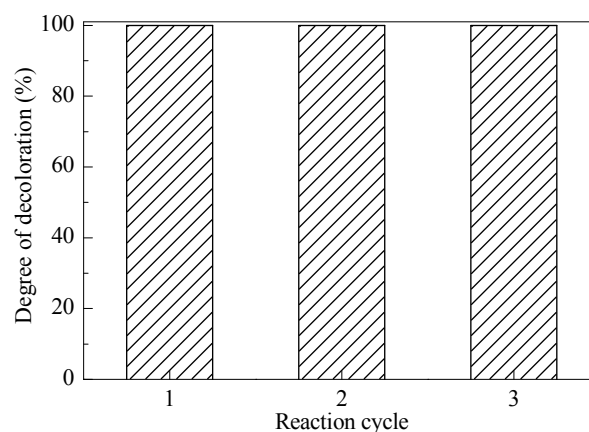


**Fig. 13.** Recyclability of CoFe<sub>2</sub>O<sub>4</sub>/CdS nanocomposite. Experimental conditions: [MB] = 25 mg/L, [nanocatalyst] = 0.5 g/L, [H<sub>2</sub>O<sub>2</sub>] = 30 mmol/L, 25 °C.

higher sonocatalytic performance [18,22,54,55]. The electrons in the CB react with H<sub>2</sub>O<sub>2</sub> to produce highly reactive •OH, which can degrade MB. The generated holes oxidise OH<sup>-</sup> ions (or H<sub>2</sub>O<sub>2</sub> molecules) adsorbed on the surface of the CdS particles to produce •OH, which indirectly degrade the organic pollutants in aqueous solution. Finally, the active species oxidise the dye molecules to the degradation products (e.g., CO<sub>2</sub>, H<sub>2</sub>O) [56–61]. Based on the above results, a mechanism of the sonogenerated electron-hole separation process in the presence of CoFe<sub>2</sub>O<sub>4</sub>/CdS is proposed and illustrated in Fig. 14. It is known that the CB of CoFe<sub>2</sub>O<sub>4</sub> is more positive than that of CdS, and its VB is also positive when compared with that of CdS [18,54,62,63]. Hence, CoFe<sub>2</sub>O<sub>4</sub> can act as a sink for the sonogenerated electrons, whereas CdS can act as an acceptor for the sonogenerated holes in the hybrid sonocatalyst [18,54].

To confirm the above-proposed mechanism, trapping experiments were conducted to determine the main active oxidant species. Upon addition of 10 and 20 mmol/L *tert*-butyl alcohol (*t*-BuOH), as a scavenger of •OH, the degradation efficiency of MB considerably decreased, and only 40% and 30% of MB was degraded, respectively, after 5 min irradiation. These results indicate that •OH radicals are the primary oxidant in the

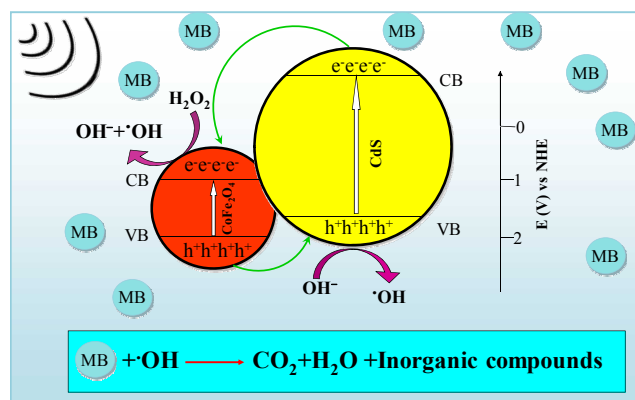


**Fig. 14.** Schematic drawing the separation of generated electrons and holes on the interface of the CoFe<sub>2</sub>O<sub>4</sub>/CdS nanocomposite under ultrasonic irradiation.

degradation of the dyes studied.

#### 4. Conclusions

A CoFe<sub>2</sub>O<sub>4</sub>/CdS nanocomposite (with a particle diameter of ~20 nm and specific surface area of 39.329 m<sup>2</sup>/g) was successfully synthesised by a simple hydrothermal reaction. Magnetic measurements revealed that the CoFe<sub>2</sub>O<sub>4</sub>/CdS nanocomposite displayed a ferromagnetic behaviour that allowed easy separation of the nanocomposite from aqueous solutions. Over the CoFe<sub>2</sub>O<sub>4</sub>/CdS nanocomposite, rapid degradation of MB, RhB, and MO dyes was observed to complete within 5, 5, and 9 min, respectively, under ultrasound and in the presence of H<sub>2</sub>O<sub>2</sub> as a •OH source. Furthermore, comparison studies revealed that the prepared nanocomposite had a higher sonocatalytic activity than pure CdS. This study presents a green, low-cost, simple, and rapid procedure for the degradation of dye pollutants in aqueous wastewater solutions.

#### Acknowledgments

The authors gratefully acknowledge the Lorestan University and Iran Nanotechnology Initiative Council (INIC) for their financial support.

#### References

- [1] A. Datta, A. Priyam, S. N. Bhattacharyya, K. K. Mukherjea, A. Saha, *J. Colloid Interface Sci.*, **2008**, 322, 128–135.
- [2] M. W. Xiao, L. S. Wang, Y. D. Wu, X. J. Huang, Z. Dang, *Nanotechnology*, **2008**, 19, 015706/1–015706/7.
- [3] Y. Wang, Y. Wang, Y. L. Meng, H. M. Ding, Y. K. Shan, X. Zhao, X. Z. Tang, *J. Phys. Chem. C*, **2008**, 112, 6620–6626.
- [4] R. Darvishi Cheshmeh Soltani, A. R. Khataee, M. Safari, S. W. Joo, *Int. Biodeteriorat. Biodegrad.*, **2013**, 85, 383–391.
- [5] R. Darvishi Cheshmeh Soltani, A. Rezaee, A. R. Khataee, *Ind. Eng. Chem. Res.*, **2013**, 52, 14133–14142.
- [6] R. Darvishi Cheshmeh Soltani, A. Rezaee, A. R. Khataee, M. Safari, *J. Ind. Eng. Chem.*, **2014**, 20, 1861–1868.
- [7] A. R. Khataee, S. Fathinia, M. Fathinia, Y. Hanifehpour, S. W. Joo, B. Soltani, *Curr. Nanosci.*, **2013**, 9, 780–786.
- [8] M. Y. Zhu, D. H. Meng, C. J. Wang, J. Di, G. W. Diao, *Chin. J. Catal.*, **2013**, 34, 2125–2129.
- [9] J. J. Yan, K. Wang, H. Xu, J. Qian, W. Liu, X. W. Yang, H. M. Li, *Chin. J. Catal.*, **2013**, 34, 1876–1882.
- [10] K. L. Lü, J. G. Yu, K. J. Deng, J. Sun, Y. X. Zhao, D. Y. Du, M. Li, *J. Hazard. Mater.*, **2010**, 173, 539–543.
- [11] J. G. Yu, W. G. Wang, B. Cheng, B. L. Su, *J. Phys. Chem. C*, **2009**, 113, 6743–6750.
- [12] V. M. Daskalaki, M. Antoniadou, G. L. Puma, D. I. Kondarides, P. Lianos, *Environ. Sci. Technol.*, **2010**, 44, 7200–7205.
- [13] Z. Y. Gao, N. Liu, D. P. Wu, W. G. Tao, F. Xu, K. Jiang, *Appl. Surf. Sci.*, **2012**, 258, 2473–2478.
- [14] Y. Shi, H. Y. Li, L. Wang, W. Shen, H. Z. Chen, *ACS Appl. Mater. Interfaces*, **2012**, 4, 4800–4806.
- [15] Y. X. Nan, F. Chen, L. G. Yang, H. Z. Chen, *J. Phys. Chem. C*, **2010**, 114, 11911–11917.
- [16] A. Kumar, A. Singhal, *J. Mater. Chem.*, **2011**, 21, 481–496.
- [17] F. Chen, R. J. Zhou, L. G. Yang, N. Liu, M. Wang, H. Z. Chen, *J. Phys. Chem. C*, **2008**, 112, 1001–1007.
- [18] J. W. Shi, X. X. Yan, H. J. Cui, X. Zong, M. L. Fu, S. H. Chen, L. Z. Wang, *J. Mol. Catal. A*, **2012**, 356, 53–60.
- [19] J. Zhang, J. G. Yu, M. Jaroniec, J. R. Gong, *Nano Lett.*, **2012**, 12, 4584–4589.
- [20] Z. D. Meng, M. M. Peng, L. Zhu, W. C. Oh, F. J. Zhang, *Appl. Catal. B*, **2012**, 113–114, 141–149.
- [21] T. T. Yang, W. T. Chen, Y. J. Hsu, K. H. Wei, T. Y. Lin, T. W. Lin, *J. Phys. Chem. C*, **2010**, 114, 11414–11420.
- [22] H. Zhang, Y. F. Zhu, *J. Phys. Chem. C*, **2010**, 114, 5822–5826.
- [23] A. H. Ye, W. Q. Fan, Q. H. Zhang, W. P. Deng, Y. Wang, *Catal. Sci. Technol.*, **2012**, 2, 969–978.
- [24] G. C. Xie, K. Zhang, B. D. Guo, Q. Liu, L. Fang, J. R. Gong, *Adv. Mater.*, **2013**, 25, 3820–3839.
- [25] A. Roychowdhury, S. P. Pati, S. Kumar, D. Das, *Powder Technol.*, **2014**, 254, 583–590.
- [26] X. F. Cui, Y. J. Wang, G. Y. Jiang, Z. Zhao, C. M. Xu, A. J. Duan, J. Liu, Y. C. Wei, W. K. Bai, *J. Mater. Chem. A*, **2014**, 2, 20939–20946.
- [27] S. Q. Liu, M. Q. Yang, N. Zhang, Y. J. Xu, *J. Eng. Chem.*, **2014**, 23, 145–155.
- [28] E. H. Jeang, J. H. Lee, K. C. Je, S. Y. Yim, S. H. Park, Y. S. Choi, J. G. Choi, M. Treguer, T. Cardinal, *Bull. Korean Chem. Soc.*, **2004**, 25, 934–936.
- [29] X. W. Liu, Z. Fang, X. J. Zhang, W. Zhang, X. W. Wei, B. Y. Geng, *Cryst.*

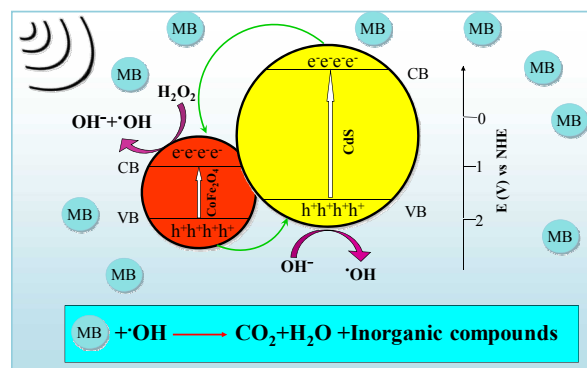
#### Graphical Abstract

*Chin. J. Catal.*, 2016, 37: 1487–1495 doi: 10.1016/S1872-2067(16)62473-7

#### CoFe<sub>2</sub>O<sub>4</sub>/CdS nanocomposite: Preparation, characterisation, and application in sonocatalytic degradation of organic dye pollutants

Saeed Farhadi\*, Firouzeh Siadatnasab  
Lorestan University, Iran

Magnetically separable CoFe<sub>2</sub>O<sub>4</sub>/CdS nanocomposite as an efficient sonocatalyst was synthesized by the hydrothermal technique and used for H<sub>2</sub>O<sub>2</sub>-assisted degradation of pollutant dyes under ultrasonic irradiation.



- Growth Des.*, **2009**, 9, 197–202.
- [30] L. Wang, H. W. Wei, Y. J. Fan, X. Gu, J. H. Zhan, *J. Phys. Chem. C*, **2009**, 113, 14119–14125.
- [31] T. H. Yu, W. Y. Cheng, K. J. Chao, S. Y. Lu, *Nanoscale*, **2013**, 5, 7356–7360.
- [32] A. Khataee, A. Karimi, S. Arefi-Oskoui, R. Darvishi Cheshmeh Soltani, Y. Hanifehpour, B. Soltani, S. W. Joo, *Ultrason. Sonochem.*, **2015**, 22, 371–381.
- [33] M. Ahmad, E. Ahmed, Z. L. Hong, W. Ahmed, A. Elhissi, N. R. Khalid, *Ultrason. Sonochem.*, **2014**, 21, 761–773.
- [34] Z. D. Meng, S. Sarkar, L. Zhu, K. Ullah, S. Ye, W. C. Oh, *J. Mater. Res.*, **2014**, 24–
- [35] L. Zhu, J. D. Chung, W. C. Oh, *Ultrason. Sonochem.*, **2015**, 27, 252–261.
- [36] Y. Wang, L. G. Gai, W. Y. Ma, H. H. Jiang, X. Q. Peng, L. C. Zhao, *Ind. Eng. Chem. Res.*, **2015**, 54, 2279–2289.
- [37] L. Zhu, S. B. Jo, S. Ye, K. Ullah, W. C. Oh, *Chin. J. Catal.*, **2014**, 35, 1825–1832.
- [38] L. Zhu, T. Ghosh, C. Y. Park, Z. D. Meng, W. C. Oh, *Chin. J. Catal.*, **2012**, 33, 1276–1283
- [39] H. P. Klug, L. E. Alexander, *X-Ray Diffraction Procedures: For Polycrystalline and Amorphous Materials*, 2nd ed., Wiley, New York, **1994**.
- [40] P. T. Zhao, K. X. Huang, *Cryst. Growth Des.*, **2008**, 8, 717–722.
- [41] B. Senthilkumar, R. Kalai Selvan, P. Vinothbabu, I. Perelshtein, A. Gedanken, *Mater. Chem. Phys.*, **2011**, 130, 285–292.
- [42] K. K. Senapati, C. Borgohain, P. Phukan, *Catal. Sci. Technol.*, **2012**, 2, 2361–2366.
- [43] F. Duan, Y. Zheng, M. Q. Chen, *Appl. Surf. Sci.*, **2011**, 257, 1972–1978.
- [44] Y. Q. Shi, K. Q. Zhou, B. B. Wang, S. H. Jiang, X. D. Qian, Z. Gui, R. K. K. Yuen, Y. Hu, *J. Mater. Chem. A*, **2014**, 2, 535–544.
- [45] J. B. Silva, W. de Brito, N. D. S. Mohallem, *Mater. Sci. Eng. B*, **2004**, 112, 182–187.
- [46] T. Harifi, M. Montazer, *Sep. Purif. Technol.*, **2014**, 134, 210–219.
- [47] S. Singh, N. Khare, *RSC Adv.*, **2015**, 5, 96562–96572.
- [48] J. Z. Yang, J. W. Yu, J. Fan, D. P. Sun, W. H. Tang, X. J. Yang, *J. Hazard. Mater.*, **2011**, 189, 377–383.
- [49] N. Ertugay, F. N. Acar, *App. Surf. Sci.*, **2014**, 318, 121–126.
- [50] Y. L. Pang, A. Z. Abdullah, *Appl. Catal. B*, **2013**, 129, 473–481.
- [51] Y. L. Pang, A. Z. Abdullah, S. Bhatia, *Desalination*, **2011**, 277, 1–14.
- [52] M. A. Alavi, A. Morsali, S. W. Joo, B. K. Min, *Ultrason. Sonochem.*, **2015**, 22, 349–358.
- [53] L. H. Ai, C. H. Zhang, L. L. Li, J. Jiang, *Appl. Catal. B*, **2014**, 148–149, 191–200.
- [54] N. Zhang, Y. H. Zhang, X. Y. Pan, M. Q. Yang, Y. J. Xu, *J. Phys. Chem. C*, **2012**, 116, 18023–18031.
- [55] L. Jia, D. H. Wang, Y. X. Huang, A. W. Xu, H. Q. Yu, *J. Phys. Chem. C*, **2011**, 115, 11466–11473.
- [56] Y. Segura, R. Molina, F. Martinez, J. A. Melero, *Ultrason. Sonochem.*, **2009**, 16, 417–424.
- [57] M. H. Entezari, Z. S. Al-Hoseini, *Ultrason. Sonochem.*, **2007**, 14, 599–604.
- [58] J. Saien, H. Delavari, A. R. Solymani, *J. Hazard. Mater.*, **2010**, 177, 1031–1038.
- [59] F. J. Zhang, J. Liu, M. L. Chen, W. C. Oh, *J. Korean Ceram. Soc.*, **2009**, 46, 263–270.
- [60] X. W. Zhang, M. H. Zhou, L. C. Lei, *Carbon*, **2005**, 43, 1700–1708.
- [61] F. J. Zhang, M. L. Chen, K. Zhang, W. C. Oh, *Bull. Korean Chem. Soc.*, **2010**, 31, 133–139.
- [62] L. Kong, Z. Jiang, T. C. Xiao, L. F. Lu, M. O. Jones, P. P. Edwards, *Chem. Commun.*, **2011**, 47, 5512–5514.
- [63] L. Zhang, Y. M. He, P. Ye, Y. Wu, T. H. Wu, *J. Alloys. Compd.*, **2013**, 549, 105–113.